SPACE ROBOTS

Cooperative robotic exploration of a planetary skylight surface and lava cave

Raúl Domínguez[1], Carlos Pérez-del-Pulgar[2]*, Gonzalo J. Paz-Delgado[2], Fabio Polisano[3], Jonathan Babel[1], Thierry Germa[4], Iulia Dragomir[5], Valérie Ciarletti[6], Anne-Claire Berthet[4], Leon Cedric Danter[1], Frank Kirchner[1,7]

Exploration of lava caves on the surface of planetary bodies near Earth is of high importance for scientific research and space exploration. The natural shielding that these caves offer against radiation and small meteorites makes them well suited for preserving exobiological signatures and protecting human-made facilities. The use of a robot team arises as the safest and most cost-efficient way to explore extraterrestrial lava caves because they are difficult to access. Although the approach has been demonstrated in similar scenarios on Earth, its adaptation to space conditions needs further research. Here, we define a lava cave exploration mission concept, including four mission phases that are performed by a heterogeneous team of three robots equipped with the required hardware and software. This mission concept was validated in a relevant scenario, a lava cave on Lanzarote island (Spain), where the team of robots was able to build a three-dimensional model of the surrounding area and skylight, introducing a scout rover through rappelling and exploring the inner part of the cave. The results obtained demonstrate the proposed mission concept's feasibility, including three next-generation planetary exploration rovers that were coordinated to obtain meaningful information about the lava cave's external and internal morphology.

INTRODUCTION

Since 1958, more than 250 spacecraft have left Earth to explore other planets, moons, and small bodies of our solar system. Most of these missions operated their scientific instruments in orbit or on the surface using rovers (*1*). As a result, the atmospheres and surfaces of these bodies have been observed repeatedly, whereas little is still known about their subsurfaces. Yet, beneath the surface, we must seek answers to a number of scientific questions about the formation and geological evolution of the landing site through processes such as volcanism, tectonics, weathering, erosion, mass loss and deposition and the potential existence of exobiological signatures sought in habitats sheltered from harsh surface conditions (*2*). However, access to the subsurface is extremely challenging. Lava tube skylights are promising gateways to the subsurface, capturing attention not only for their scientific importance but also for practical space exploration perspectives (*3*). Lava tubes have been considered candidate locations for future human outposts because they provide protection from dangerous radiation, extreme temperatures, dust storms, and micrometeorite impacts (*4*). Several lava tubes have already been identified from orbits on Mars (*5*) and the Moon (*6*). However, there are now no missions to send humans to explore these locations because of the great difficulty and risk that such a mission would entail.

Nevertheless, lava tube exploration is relevant and challenging not only on remote planets but also on Earth. Recent and older lava tubes have been thoroughly investigated to analyze microbial communities, even finding previously unknown species (*7*). Recent volcano eruptions have created lava tubes, which can provide insight into how life arises in such extreme conditions. The same conditions make lava tubes impossible for humans to explore. An example is the Cumbre Vieja eruption (La Palma, Spain) in 2021, which generated lava caves that are yet to be explored because of the extreme temperature and chemical environment inside (*8*).

To address lava tube exploration in remote planets, a robotic mission is safer and more cost-effective than involving astronauts. From Earth, robots can be teleoperated through a commanding and monitoring station (CMS), especially while performing surface operations. However, in subsurface operations, communication constraints arise, requiring increased autonomy of the robot. The Defense Advanced Research Projects Agency (DARPA) subterranean challenge is an example of how complex underground robotic navigation is. Although the challenge was conceived to promote related technology development to support underground operations for first responders, there is a strong similarity to the exploration of lava caves. This challenge reflected the complexity of this type of mission and the factors that affect the probability of success. On the basis of the results of this challenge (*9*), a heterogeneous robot team was identified as the most advantageous option compared with a single rover, a homogeneous team, or a swarm. Unlike using a single rover, using a team provides redundancy and enhances the mission's capabilities. With respect to a homogeneous robotic team or swarm, the different required tasks can be tailored to systems with specific capabilities, allowing concurrent execution of operations while minimizing payloads and thus increasing overall efficiency. The advantages of heterogeneous robotic teams in scientific surveys of planet surfaces have previously been proposed (*10*–*12*). In work from ETH Zürich (*12*), a team of quadrupeds, each equipped with different sensors and actuators, cooperated to maximize the acquisition of scientific data, making the most efficient use of the team's energy and time. In addition, NASA Jet Propulsion Laboratory proposed the exploration of lava caves using a heterogeneous team of two-legged robots (*13*).

[1]Robotics Innovation Center, German Research Center for Artificial Intelligence (DFKI), Robert-Hooke-Str. 1, 28359 Bremen, Germany. [2]Space Robotics Laboratory, Universidad de Málaga, C/Dr. Ortiz Ramos, Málaga, Spain. [3]Space Applications Services, Zaventem, Belgium. [4]Magellium, Ramonville Saint Agne, France. [5]GMV Aerospace and Defence S.A., C/Isaac Newton, 11 Tres Cantos, Madrid, Spain. [6]LATMOS/IPSL, UVSQ Université Paris-Saclay, Sorbonne Université, CNRS, Guyancourt, France. [7]Faculty of Mathematics and Computer Science, University of Bremen, Bibliothekstrasse, 1, Bremen, Germany.
*Corresponding author. Email: carlosperez@uma.es

Here, we propose a mission concept for robotic exploration of lava tubes or extremely inclined surfaces using a tether, illustrated in Movie 1. It is divided into four mission phases (MPs): mission phase 1 (MP-1), cooperative exploration and mapping of the area surrounding the lava tube skylight; mission phase 2 (MP-2), skylight exploration with a sensorized payload cube that is ejected down into the lava cave; mission phase 3 (MP-3), cooperative rappelling of a scout rover through the skylight; and mission phase 4 (MP-4), lava cave exploration and three-dimensional (3D) representation.

Compared with similar approaches (*14*, *15*), this concept has two main advantages. First, we generated a detailed representation of the surface and the highly inclined region before the tethered descent. This ensures that only areas that can feasibly be traversed are attempted and that the complexity of autonomous navigation during the controlled descent can be reduced. This information can become crucial, because the range of motion of tethered systems is limited by their attachment points and the gravity vector (*16*). The second advantage is that the cave exploration rover can release its attachment to the tether, communication, and power supply system, such that navigation inside the cave can be done more flexibly.

RESULTS

Heterogeneous robot team

The heterogeneous team of robots is depicted in Fig. 1A and described in detail in Movie 1. It was composed of three robots: SherpaTT (*17*), Coyote III (*10*), and the Lunar Volatile Mobile Instrumentation (LUVMI-X) (*18*). SherpaTT performed surface exploration and supported the tethering operation. Coyote III (*10*) provided subsurface exploration capability and was able to rappel down the skylight into the lava tube. Last, LUVMI-X explored the surface and was equipped with a payload launcher to analyze the skylight.

Figure 1B shows the various capabilities of the robots. First, SherpaTT (fig. S2) is a hybrid wheeled-legged rover with a variable footprint and full Ackermann steering that weighs ~210 kg when fully equipped. The rover is extended with an external avionics box, which is used to provide autonomous navigation and mapping capabilities using representative electronic components for space. SherpaTT features a robotic manipulator with six degrees of freedom (DoFs). The maximum payload of 25 kg in Earth gravity is limited by the spherical wrist joints. Its mechanical features make it suitable for carrying and deploying the required payloads, as well as for acting as a mobile anchor during the rappel operation.

The second rover involved in this mission is Coyote III (fig. S3). It is a small rover with low weight (~20 kg) and high mobility, which makes it suitable for rappelling and exploring narrow lava tubes. It has skid-steering locomotion with four wheels and a passive joint for the back-wheel axis, which improves the system's stability over terrain irregularities. Coyote III is also equipped with a ground-penetrating radar (GPR), providing the ability to explore the subsurface to find lava tubes. To perform rappelling, a tether management and docking system (TMDS) was designed to include the tether that connects SherpaTT and Coyote III. The tether is rolled on an actuated spool inside the TMDS to control the winding (and unwinding) velocity. In addition to being used as a rope to rappel Coyote III down the skylight, the tether also transmits power and data from SherpaTT to the TMDS to command its actuators. Additionally, this link can be used to provide energy to Coyote III inside the lava tube and to communicate between the rovers.

Last, LUVMI-X (fig. S4) is a lightweight and cost-effective rover conceived to investigate the resource potential of lunar volatiles. It can perform autonomous navigation and mapping in collaboration with SherpaTT to explore the area surrounding the skylight. The LUVMI-X design enables the rover to carry a set of configurable payloads based on the scientific nature of the mission. For this mission, LUVMI-X was equipped with a sensorized payload cube and a launcher to eject the payload into the skylight.

Analog field trial

To demonstrate the feasibility of the proposed approach and the robot team, a field test was performed on the volcanic island of Lanzarote, Spain. The selected skylight is part of the extensive La Corona lava tube network, located in the northern part of the island. The field test campaign had a duration of 21 days. During this time, the different subsystems were tested onsite, and at the end of the field test period, a final demonstration was performed in which the four MPs were executed in the planned sequence. Movie 2 shows the results obtained from the analog field test on Earth, which are described below.

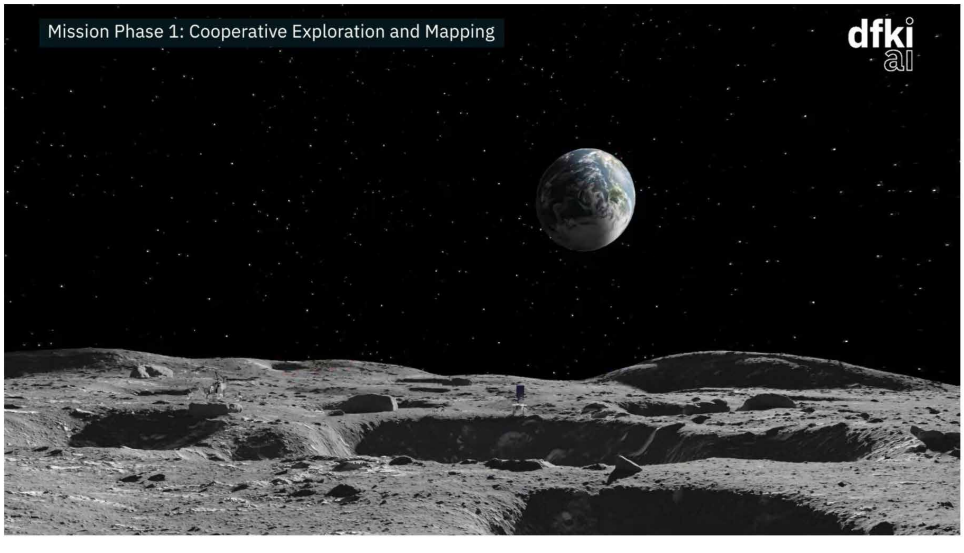

Movie 1. Video that recreates the proposed mission concept on the Moon.

MP-1—Cooperative exploration and mapping

The first MP aimed to collaboratively explore the area around the skylight and produce a digital representation of the environment. For this purpose, the area to be explored was divided into two sections that were assigned to SherpaTT and LUVMI-X according to their initial position. The robots covered these areas, obtaining images from each waypoint and generating a joint map of the surface. Along with the total area to be explored, a reference locomotion speed was assigned to each rover. A lava tube characterization was attempted using the GPR data

gathered by Coyote III. A visualization of the test area is provided in Fig. 2B.

SherpaTT explored the largest area given its coverage, fusing sensor data from the avionics box and the rover. SherpaTT used a stereo bench composed of Basler acA2040-25gmNIR cameras to obtain its part of the map. LUVMI-X explored a medium-sized area using Stereolabs' ZED sensor, which directly provides depth information. Both systems had navigation cameras (NavCams) located on a pan-tilt unit at the top of a mast. In parallel, Coyote III inspected the surface area crossing the lava tube by taking GPR measurements every 10 cm to create a complete profile. On the three rovers, wheel and visual odometry were fused to obtain the localization. The backbone functionality of navigation was provided by the guidance and control component, which took the rover to the exploration waypoints. The waypoints were generated onboard by the mission management component.

The integrated exploration components were refined on each rover separately during the field test, resulting in a reduction of the localization error and a more precise trajectory control. After addressing the technical challenges of time synchronization of heterogeneous hardware components and communication, it was possible to run two tests of fully integrated cooperative exploration, where the first one served to correct an error in the orientations used to match the different rover maps into the unified one.

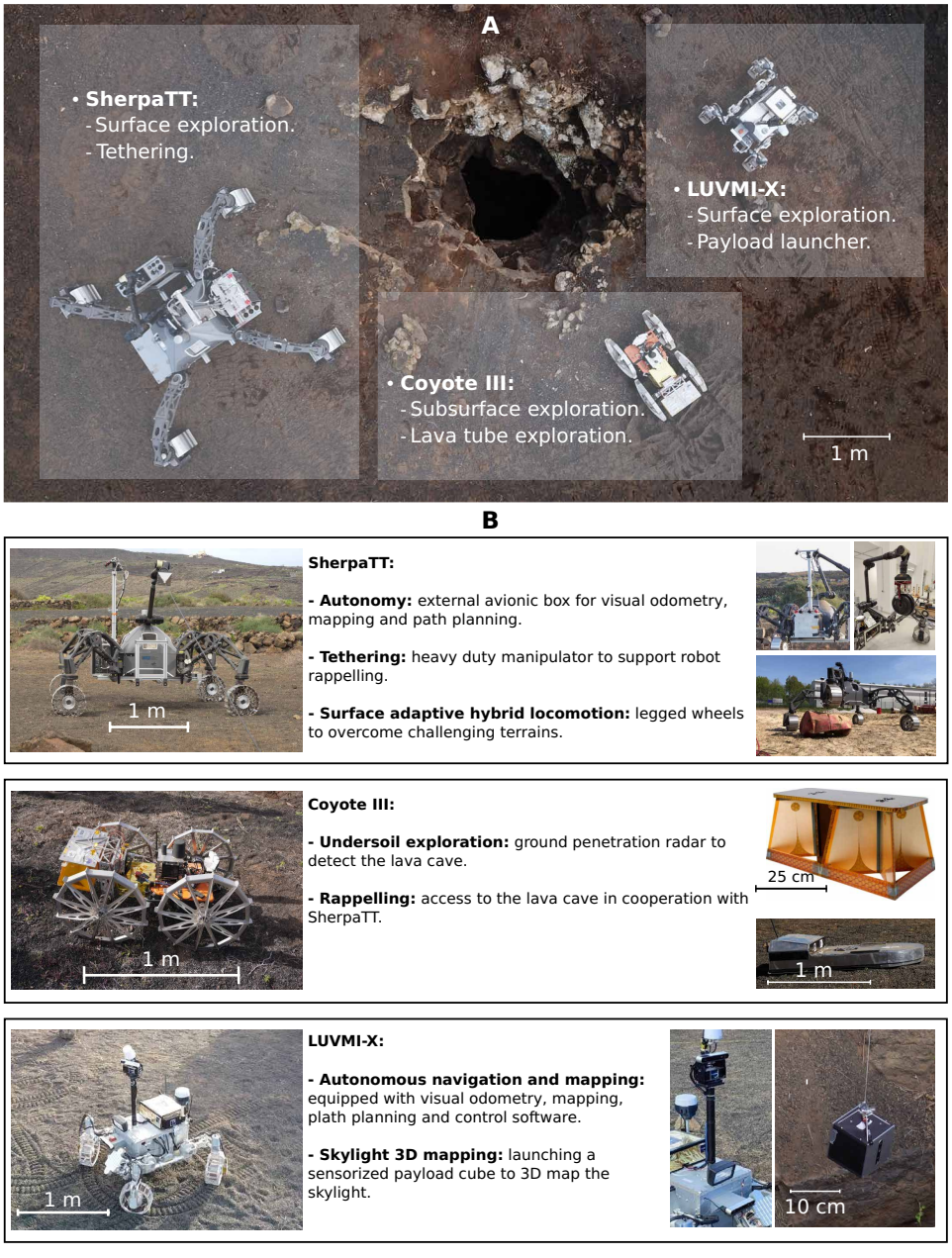

Fig. 1. Robot team used during the Lanzarote field trial along with scale bar. (**A**) Heterogeneous robot team. (**B**) Robot capabilities and used materials.

In the second fully integrated test, SherpaTT explored the northern area around the skylight, roughly 900 m^2, in 15 min. Coyote III explored a trajectory of 3 m, gathering and forwarding datagrams captured every 10 cm within 20 min. Last, LUVMI-X explored the southern area around the skylight, roughly 400 m^2, in 25 min. Digital elevation model (DEM) generation and path-planning routines required SherpaTT and LUVMI-X to stop their base motion after each trajectory. The rover's commanded speed was set to 10 cm/s for SherpaTT and LUVMI-X and to 5 cm/s for Coyote III. Coyote III performed stops every 2 s for GPR data acquisition.

The exploration waypoints, cooperative map, and the localizations produced by the visual odometry component on SherpaTT and LUVMI-X are shown in Fig. 2A. Two independent sources were used to analyze the quality of these data products: differential GPS, captured onboard the rovers, and a georeferenced drone map, produced with commercial hardware (DJI Mavic Pro) and software (Pix4D Mapper). The mean error of the points of the map was 0.298 m with an SD of 0.179 m. A visualization of this evaluation is presented in Fig. 2C. The localization had a Z component (i.e., height estimation) mean signed error of 0.133 m on SherpaTT and −0.126 m on LUVMI-X, as shown in Fig. 2D. These oppositely signed errors explain the height differences in the cooperative map when comparing the regions covered by SherpaTT and LUVMI-X.

The tests in this phase achieved the goal of exploring and mapping the area with the accuracy needed to determine the position from which to perform the payload cube ejection. The map was also accurate enough to be used to identify candidate paths for the first part of the rappelling. Unfortunately, during the field

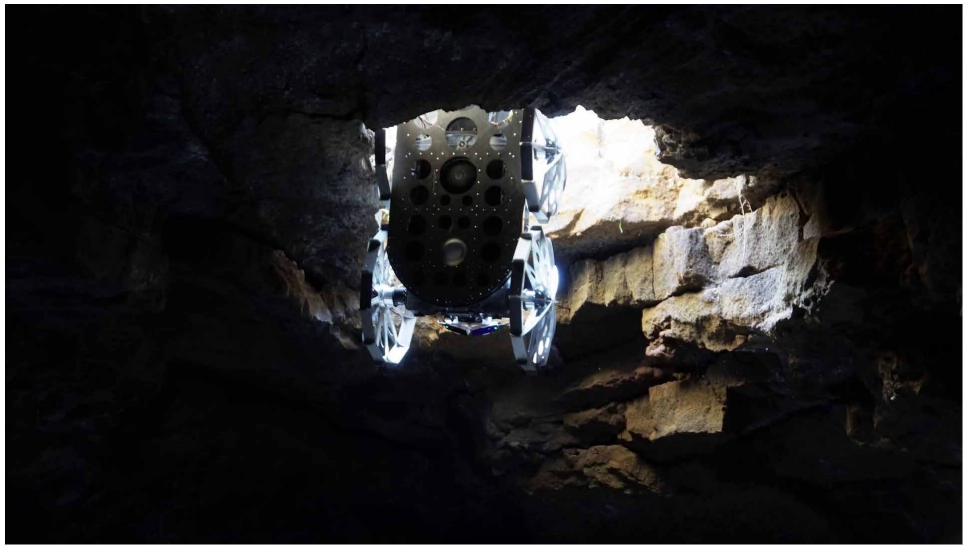

Movie 2. Obtained results for each mission phase.

test campaign, unexpected moisture at the surface and in the shallow subsurface largely degraded the GPR's ability to probe the subsurface and detect the top of the lava tube. Because of rainfall, the conductivity of the shallow subsurface was much higher than expected, resulting in substantial losses affecting the amplitude of the radar waves. Figure S1 shows two images (called radargrams) generated from data acquired by the same GPR in two different environments. The radargram in fig. S1A, obtained in a frozen environment (therefore, in fairly favorable conditions because of the absence of liquid water) during a field test campaign in Svalbard (*19*), demonstrates the ability to detect a buried cave with a GPR. In fig. S1B, for comparison, a radargram acquired during a traverse over the lava tube in the Lanzarote field test is shown. Eventually, a weak signal, not coming from the surface, was visible at a depth of about 4 m and could correspond to the top of the lava tube. Given the weakness of the signal in question, it could also be interpreted as a reflection coming from a large buried rock.

MP-2—Skylight exploration with payload cube

The objective of the second phase was to characterize the lava tube skylight using an ejectable sensorized cube, which provided necessary information for successful rappelling in the third MP. This information included a map of the skylight and an estimation of the diameter and roughness of the bottleneck, or smallest area of the skylight, to understand the best side to approach the descent. For this purpose, we designed a sensorized (payload) cube equipped with two RGB-D cameras for mapping and a fisheye stereo RGB camera for visual odometry. The payload cube also included an onboard computational unit to process and register the data coming from the sensors and an IP-Mesh–based communication module to transmit the data collected back to the LUVMI-X rover while descending.

The demonstration of this phase took place in two stages. During the first stage, LUVMI-X was teleoperated to approach the skylight and shot, using a spring-based ejecting system, a nonsensorized mock cube. This stage demonstrated the feasibility of an autonomous deployment by ejecting the payload cube inside the lava tube as shown in Fig. 3A. During the second phase, a structure was mounted over the skylight access, with a pulley system capable of emulating different gravity levels when the sensorized payload cube was descending through the lava tube (Fig. 3B). The division into two stages was needed for multiple reasons. First, the sensors of the cube would not have survived the fall at Earth's gravity, making the experiment not replicable. Second, the descent of the cube with Earth's gravity would have been faster, which would not represent the scenario and the data that the payload was intended to collect. Last, legal regulations regarding the maximum ejection joules for the system to be classified as a weapon limited the maximum range of the ejection system. Together, it was thus representative to demonstrate the descent using the pulley system.

The sensorized cube was successfully lowered at representative accelerations around 1.6 m/s^2 using a velocity-controlled motor and the MotionLab software suite. It collected 3D point clouds from the RGB-D cameras and a pose estimation from the visual odometry module. These data were transmitted back to LUVMI-X and the CMS, where higher computational resources were available to process them. A mapping pipeline was implemented to filter the local 3D readings and then merge them into a fixed frame using a position output that combined the visual odometry output with a singular value decomposition–based iterative closest point (ICP) algorithm.

The final result produced at this phase was a 3D reconstruction of the skylight (Fig. 3C). An analysis of the inner convex hull of slices of the lava tube at different heights showed that the bottleneck of the analog lava tube access in Lanzarote was 2.65 m down the entrance. This analysis also provided the bottleneck minimum diameter, which was estimated at 1.85 m, against the manually measured 1.65 m. This analysis is represented in Fig. 3C, where red and orange lines represent the bottleneck. Normal-based segmentation analysis, together with analysis of the curvature of the lava tube point cloud, provided important information regarding the roughness of the entrance, allowing the identification of the best access point for the rappelling in MP-3. Figure 3D shows the final 3D representation of the skylight with Coyote III placed at the best entrance.

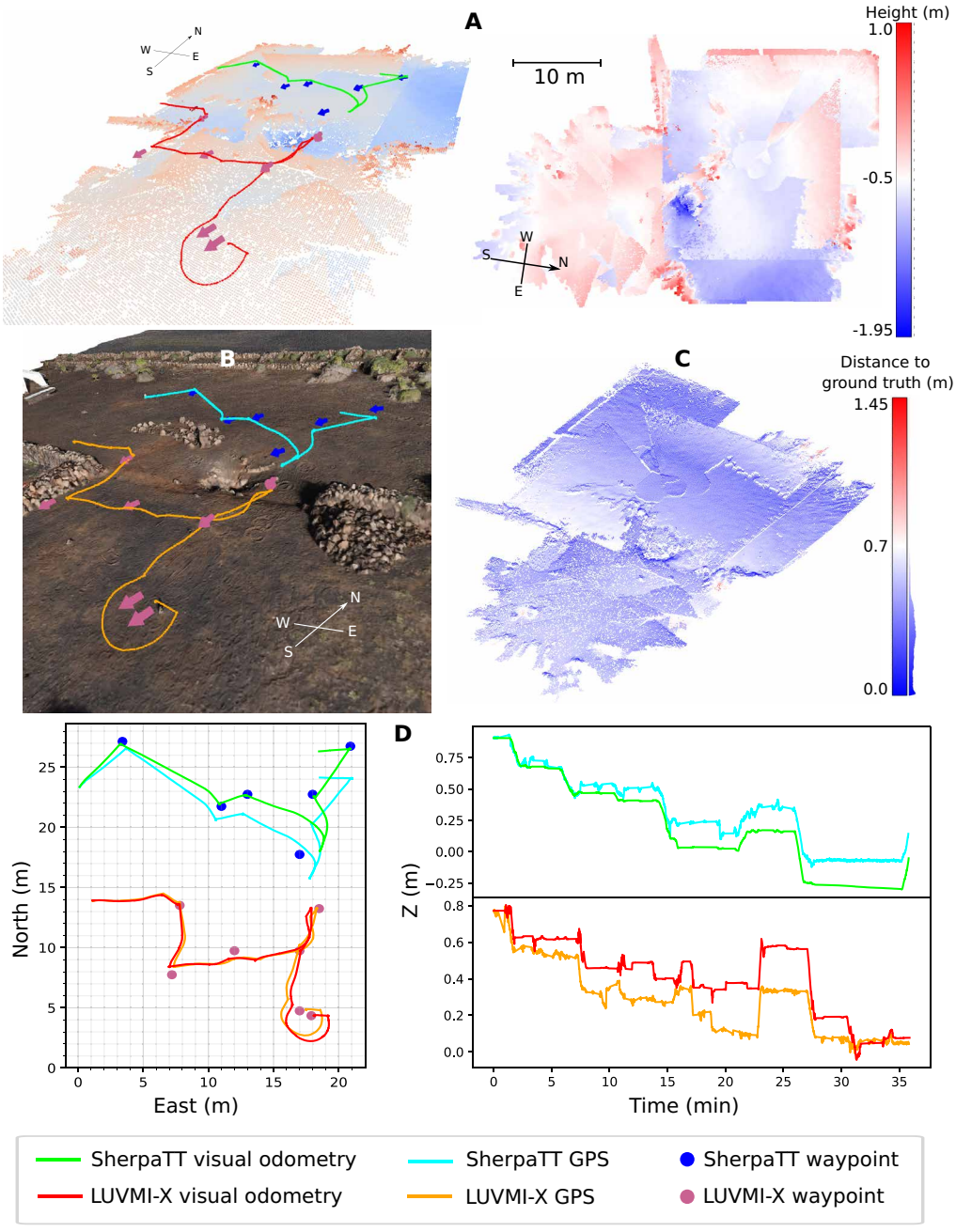

Fig. 2. Cooperative exploration and mapping by SherpaTT and LUVMI-X, MP-1. (**A**) Cooperative map, visual odometry, and exploration way points. (**B**) Ground truth of the test area. (**C**) Cooperative map deviation. (**D**) Visual odometry deviations.

MP-3—Rappelling into the lava tube

The goal of MP-3 was to get Coyote III inside the lava tube by rappelling into the skylight. The operators selected the most suitable access point for the rappelling, and SherpaTT was commanded to place itself at the correct position to start the rappelling. Once positioned, SherpaTT deployed the TMDS with its six-DoF manipulator (*20*). The deployment trajectory was determined in advance through manipulator poses at intermediate waypoints, and the motion between the waypoints was planned and executed online. Coyote III initiated the docking process with the TMDS as shown in Fig. 4A. Coyote III autonomously detected the TMDS, drove backward onto it, and attached to it, in some cases requiring remote control assistance for the approaching phase. Once attached, a power and data connection chain between SherpaTT, the TMDS, and Coyote III was established via the tether. Then, Coyote III drove toward the skylight, starting the descent into the lava tube, whereas SherpaTT served as a mobile anchor supporting the rappel with its manipulator. Figure 4B shows the rover entering the lava cave successfully. For this purpose, an autonomous guidance component synchronized the driving speed of the rover and the release speed to keep

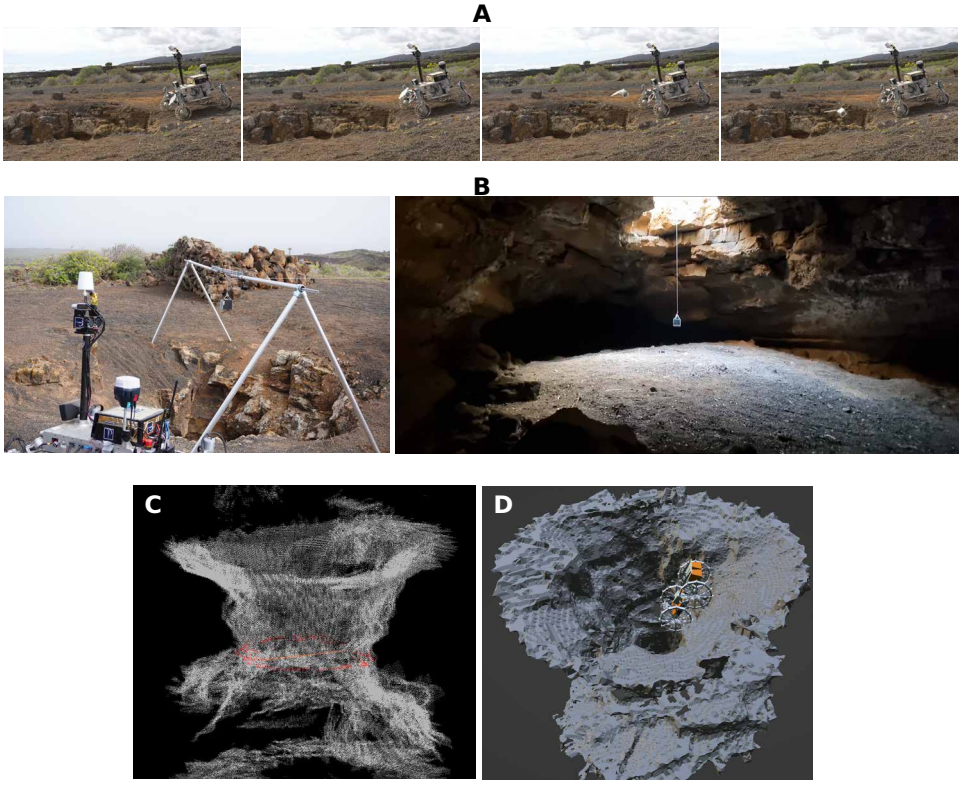

Fig. 3. Results of the skylight exploration with the payload cube during MP-2. (**A**) Payload cube launching. (**B**) Pulley system to emulate different gravity. (**C**) Obtained point clouds where the minimum diameter was estimated. (**D**) Skylight 3D representation with the best rover entrance.

the tether under controlled tension. Besides, given the considerable combined weight of Coyote III and the TMDS, a model predictive controller (MPC) for SherpaTT coordinated the rover-manipulator motions depending on the measured forces on the arm's end effector, so the main efforts were absorbed by the bigger joints of the manipulator; thus, the smaller joints were relieved to avoid damage. Last, Coyote III landed on the lava tube floor, which was detected on the basis its pitch, and undocked from the TMDS, marking the end of the rappelling (and of MP-3).

The whole MP-3 took ~8 min, of which 4 min, on average, were dedicated to the rappelling operation. Coyote III rappelled vertically for around 2 min to descend 5 m at 5 cm/s until touchdown at the bottom of the lava tube. Because Coyote III sometimes started to continuously turn axially during the vertical descent, the rover's wheels kept rolling throughout the operation. Hence, the rover advanced as soon as it touched the ground, ensuring a proper landing. Regarding the forces endured by SherpaTT's robotic arm, the MPC was able to modify the rover configuration (base and arm joint positions) to keep the torques below the joints' limits, with the manipulator's last link finishing always aligned with the tether. Movie S1 shows how the torques were reduced by coordinating the rover and arm motions, and Fig. 4C shows the obtained torques from each manipulator joint, where all of them were within the torque limits (red dashed line). Last, the TMDS was demonstrated to be robust enough during the whole MP-3, ensuring a firm dock with Coyote III, unwinding the tether at the desired velocity without entanglements in the spool, and providing power and data to Coyote III after the touchdown.

MP-4—Lava tube exploration with Coyote III

The objective of MP-4 was the construction of an accurate 3D representation of the lava tube and transmission of this data product back to the CMS. For this purpose, during the field test, a first performance analysis of the locomotion and environment representation components in a lava tube was carried out.

The Coyote III locomotion capabilities were demonstrated by remote control throughout the lava cave. The cave featured vertical cross sections between 50 and 4 m in radius, with inclinations of 25° and different types of surfaces, including gravel, sand with buried rocks in the area of the skylight, and smoothly solidified (Pahoehoe) as well as rough spiny ('A'ā) consolidated lava crusts. More than 235 m were traversed in teleoperated mode inside the cave. Figure 5C shows one of the most challenging areas. Despite the narrow space and the harsh consolidated lava surface, Coyote III moved easily and was not damaged. Only some areas, including large rocks that had collapsed from the ceiling, precluded the micro rover from traversing them, blocking the access to some regions. The most dangerous locomotion maneuvers were the point turns. These had to be avoided on surfaces of consolidated, irregular rock where the friction with the wheels was high enough to block motion and, in some cases, tip over the rover, jeopardizing the mission.

For localization and mapping, Coyote III relied on a stereo bench of time-of-flight (ToF), Vzense DCAM710, cameras. In the point cloud of the ToF triplet shown in Fig. 5B, an artifact due to interference between the two ToF cameras can be observed as a blue depression in the lower right corner, and the TMDS is in red. A second ToF triplet in Fig. 5D with no defects shows an obstacle on the floor and the walls of the cave.

Although the construction of maps onboard was not possible reliably because of the artifacts generated by the interference between the two cameras, offline environment reconstructions using the gathered point clouds by Coyote III were generated. Figure 5A shows a reconstruction of the skylight produced offline using only the captured sensor data by Coyote III while performing some simple predefined motions on the landing area. Further data for environment reconstruction were collected through remote-controlled operations in different sections of the cave. During autonomous and teleoperated sessions, log data including raw sensor data and pose estimations were captured and have been made publicly available.

To assess the quality of the maps through comparison, an additional rover (Asguard v4) was brought to the field test and was used to generate a 3D point cloud of the complete cave. This

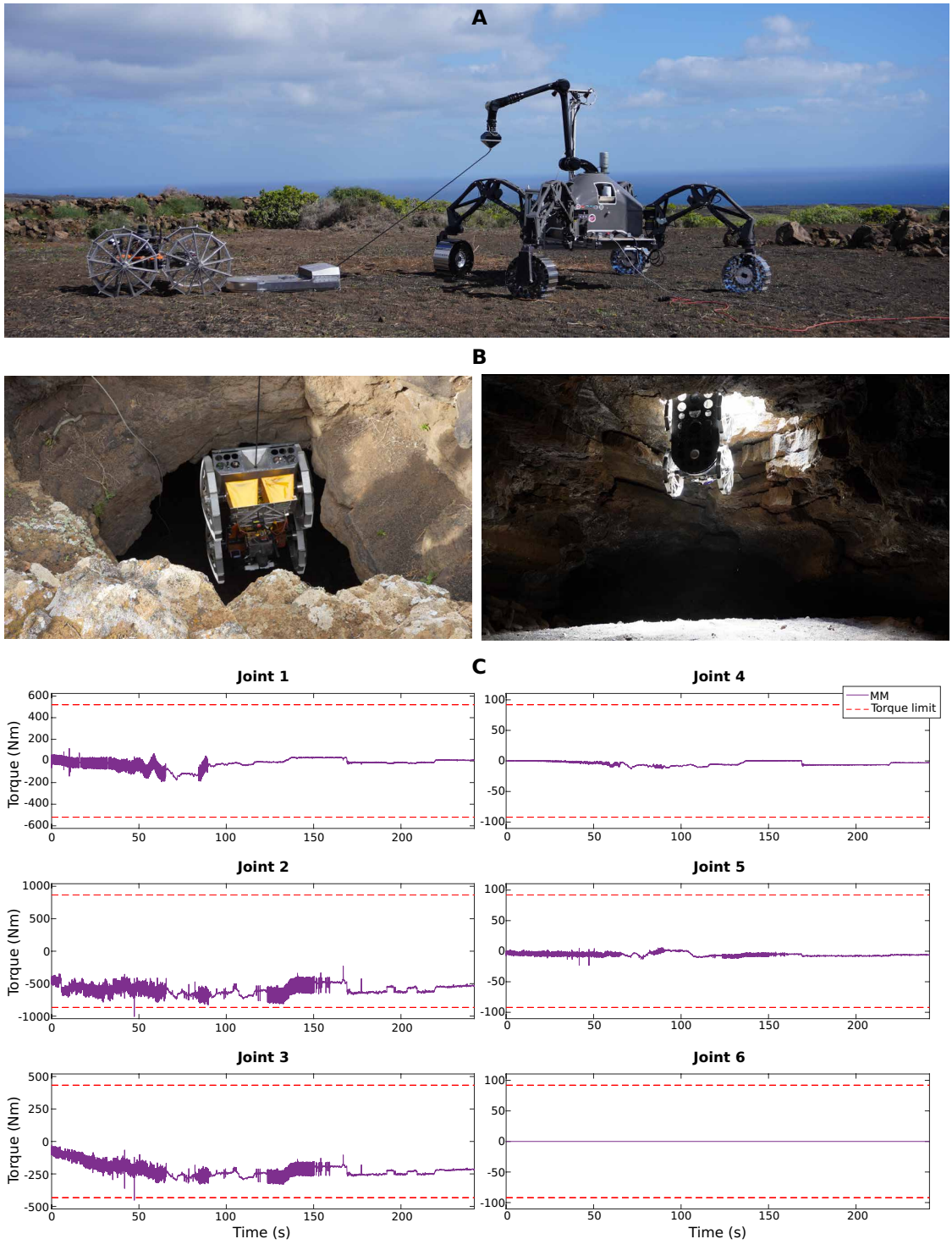

Fig. 4. Coyote III rappelling to access the skylight supported by the TMDS and SherpaTT (MP-3). (**A**) Coyote III approaching the TMDS. (**B**) Coyote III entering the cave. (**C**) Torques experienced by the SherpaTT arm during the rappelling operation.

was necessary because no ground-truth information about the cave was available. Asguard v4, previously used in a similar scenario (*21*), was equipped with a Velodyne 32 LIDAR sensor. A visual comparison between the LIDAR-based ground-truth map (Fig. 5F) and the one produced offline with the captured data by Coyote III (Fig. 5E) through remote-controlled operations is provided. It can be observed that the postprocessed cave reconstruction based on Coyote III captured data visually resembles the ground-truth reconstruction produced by Asguard v4. Although the integrated point clouds produced by Coyote III were not sufficient

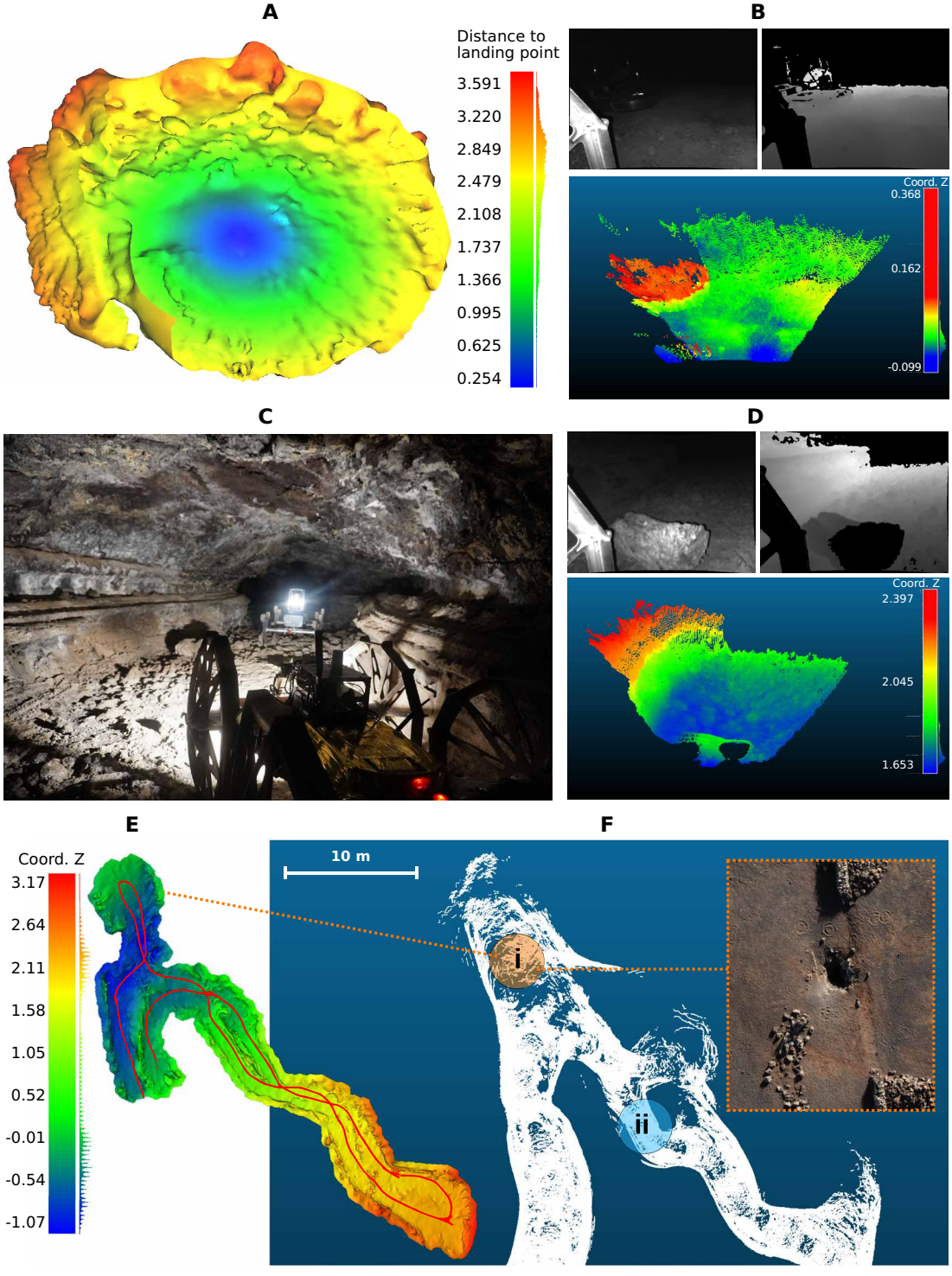

Fig. 5. In MP-4, cave reconstructions from rover data were produced and the efficient mobility of Coyote III inside the lava tube was validated. (**A**) Skylight mesh produced by Coyote III. (**B**) Skylight ToF data visualization. (**C**) Rovers traversing a narrow corridor. (**D**) Passage ToF data visualization. (**E**) Coyote III cave reconstruction. (**F**) Ground-truth rover cave reconstruction. [(F), i] Skylight area and [(F), ii] narrow corridor area.

to enable a quantitative comparison with the ground-truth or create an accurate 3D reconstruction, in the mission context, this information was useful in understanding the morphology of the lava cave.

DISCUSSION

This paper proposes the use of a heterogeneous, cooperative team of robots to access and explore a lava cave and produce 3D models of the traversed regions. For this purpose, each of the rovers assumed roles during the different MPs. The proposed approach to completing the mission was divided into four phases. Obtained results from each phase were compared against a set of key performance indicators (KPIs) that were defined at the beginning of the project, as shown in table S2.

In MP-1, SherpaTT and LUVMI-X collaborated to generate a DEM with enough accuracy to identify the skylight and place the rovers in the correct position during the following phases. The DEM was generated using visual odometry and 3D reconstruction techniques. Recent advancements in methodologies, exemplified by neural radiance fields (*22*) and Gaussian splatting (*23*), have exhibited superior performance compared with conventional approaches, such as those used in this study. Nonetheless, a notable limitation of these advanced techniques is their substantial demand for computational resources, which renders them unsuitable for onboard processing. In parallel, Coyote III was used to scan the subsurface using the onboard GPR. However, the obtained subsurface analysis results were not as expected; the terrain conductivity was too high because of its humidity, and the measurements captured by the GPR, designed for drier Mars surfaces, were not conclusive. However, this scientific instrument was previously validated in a dry surface with positive results.

During MP-2, the skylight was explored using the payload cube, which demonstrated its capacity to recreate the skylight in 3D by emulating a free fall under lunar gravity through a pulley system. Although space qualification of this system is pending, the field test was essential to validate it, getting an accurate representation of the skylight. This 3D model, combined with the DEM of MP-1, was manually analyzed to determine the entry point.

The descent of Coyote III was done in MP-3, using the SherpaTT manipulator and the TMDS to support the rappelling and activating the SherpaTT adaptive control to ensure safe tensions during the rappelling. Although gravity on Earth is higher compared with that on other planets such as Mars or on the Moon, we were able to place Coyote III in the lava cave without any damage. The force exerted on the manipulator was minimized to avoid excessive torques, and investigation is ongoing to determine how these torques would affect the manipulator in more beneficial extraterrestrial scenarios. However, it is important to highlight that this MP was done autonomously, thus avoiding possible communication delays and losses that could happen on remote planets.

Last, Coyote III detached from the TMDS and explored the lava cave in MP-4 with the objective of generating a 3D map of it. The tethering module, which can be attached and detached, is a contribution of the proposed approach. Coyote III was suitable for traversing the harsh terrain and collecting point clouds through remote control, therefore validating the locomotion and data acquisition approach. The rover could traverse the different terrains in the lava cave, although it was unable to execute point turns safely in consolidated irregular rocky surfaces because of high friction. Although other types of locomotion, such as legged, may improve performance, the aim of this test was to validate this specific rover's locomotion capability for lava cave exploration. We were able to reconstruct the morphology of the lava cave despite the limitations caused by sporadic interference between the two ToF cameras.

Autonomous navigation is desirable for this type of mission. Although a lot of advances have been made, most of them related to the DARPA subterranean challenge (*9*), we only demonstrated locomotion and mapping capabilities. Consequently, there is a need to investigate innovative methods related to localization, communications, motion planning, and control, particularly in the context of lava cave exploration in extraterrestrial environments. A primary constraint in this endeavor is the computational capacity limitation of space-qualified hardware.

In summary, a heterogeneous cooperative robot team is a promising approach to address the access and exploration of extraterrestrial lava caves. The presented analog field test showed reliable and efficient performances in most of the defined MPs. In the case of MP4, autonomous lava cave exploration remains open as a challenge that has been previously covered in the literature on Earth. However, the mission concept needs further research to be extrapolated to a real planetary exploration scenario. Nonetheless, exploration approaches that are not fully autonomous, such as the one proposed in this paper, would already provide a substantial scientific reward as long as the rover can communicate with the CMS.

MATERIALS AND METHODS

Hardware and software architecture

Figure 6 illustrates the robot team architecture, including the materials (green) and methods (orange) used, the latter commonly implemented as software components. The robots were controlled by a CMS that was connected to the mission management subsystem, which was in charge of commanding the robots through the guidance navigation and control (GNC) stack, allowing them to explore the skylight area autonomously. For this purpose, the robots were equipped with different sensors that were used for perception and localization. Moreover, each of the robots was equipped with hardware that allowed them to perform specific tasks. Coyote III was equipped with a GPR to explore the subsurface during MP-1, and it was also docked to the TMDS to perform the rappelled descent into the lava cave. SherpaTT transported and deployed the TMDS and used its manipulator to support Coyote III during the rappelling task. Last, LUVMI-X included a payload cube that was used to obtain a 3D representation of the skylight to identify suitable access routes for the rappelling.

Hardware for perception, localization, and mapping

Perception, localization, and mapping play a crucial role in rover autonomy. Commonly, an onboard computer (OBC) is required to process all the information perceived by the sensors to estimate the current pose of the rover and provide a local map of the surrounding area. Depending on the role of each rover, they were equipped with different sensors. However, most of them shared the use of cameras, inertial measurement units (IMUs), and wheel encoders. SherpaTT was equipped with an avionics box that includes two processing units: a field-programmable gate array (FPGA)–based board dedicated to

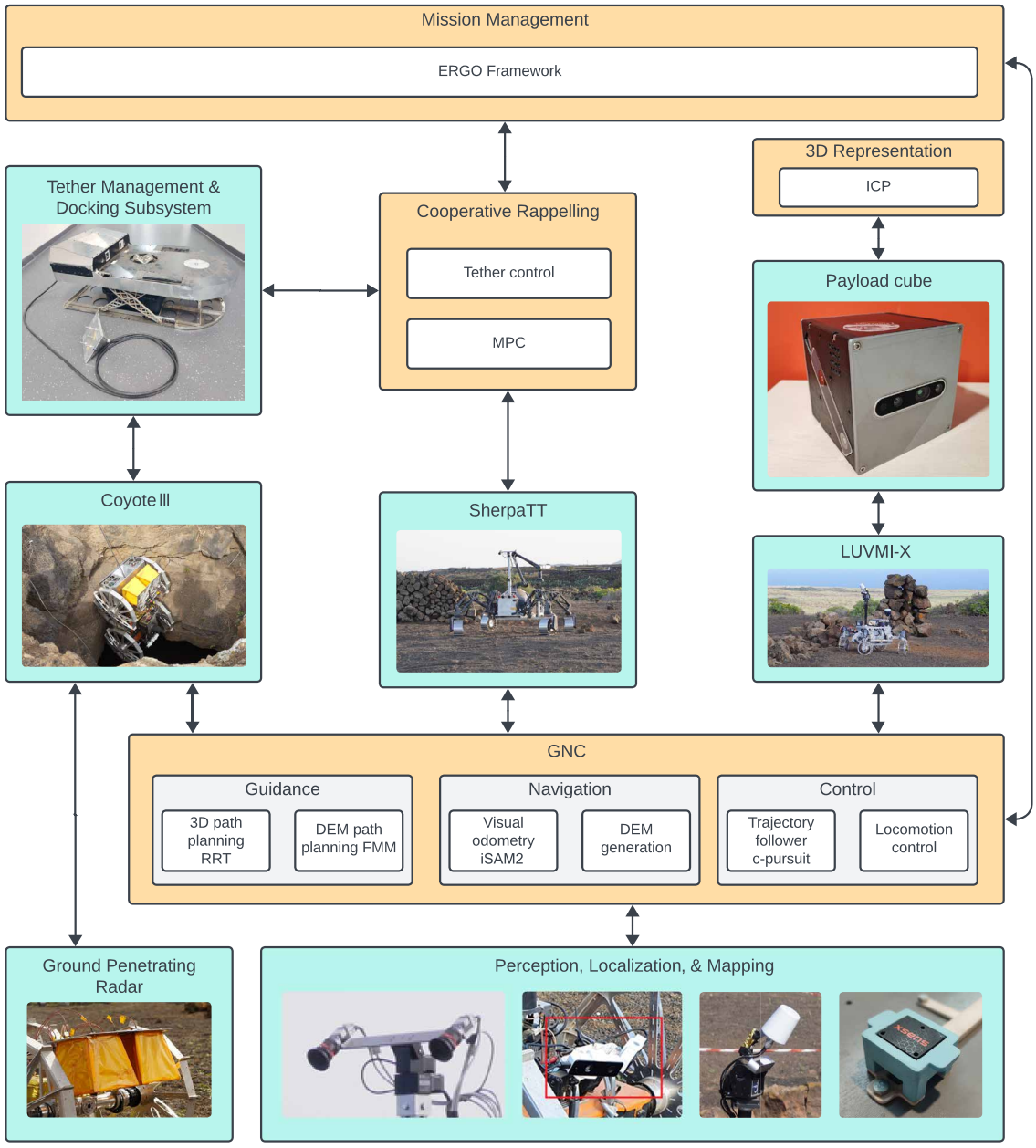

Fig. 6. Robot team architecture. The hardware (materials) and software (methods) are represented as green and orange blocks, respectively. FMM, fast marching method; RRT, rapidly random tree; c-pursuit, conservative pursuit.

the acquisition of data products for localization and a next unit of computing (NUC) computer, in which the GNC and mission management stack was deployed. Table S1 shows the mounted OBC and sensors on each rover. SherpaTT and LUVMI-X were equipped with NavCam and localization cameras (LocCams), whereas Coyote III was only equipped with a stereo bench of ToF cameras and a tiny camera for marker detection to perform the autonomous docking. The NavCams were used to perform mapping, generating a DEM from the surrounding area that will later be used to compute a local path that avoids the obstacles encountered. LocCam was used to locate the rover using visual odometry methods. Last, the IMUs were mainly used to compute the orientation (yaw, pitch, and roll) of the rovers, and acceleration measurements were fused with motor encoder information to improve localization of the rover.

Ground-penetrating radar

The GPR accommodated on Coyote III was a carbon copy of the GPR WISDOM (*24*) designed for the ExoMars rover's mission to characterize the shallow subsurface of Mars. It was mounted at the back side of Coyote III, as illustrated in Fig. 1B. This radar is capable of detecting and characterizing geological layers in the subsurface (*25*), locating embedded blocks larger than ~10 cm in three

dimensions (*26*), and statistically characterizing heterogeneous units providing the typical size of the heterogeneity (*27*). On Mars, it will allow selection of the best and safest places to collect samples in the subsurface with the mission's drill. The choices of its central frequency (1.75 GHz) and its bandwidth (2.5 GHz) were guided by the mission requirements (penetrating depth of ~2 to 3 m and vertical resolution of a few centimeters in the dry martian environment). To maximize the energy transmitted by its antennas, the GPR is a step frequency radar that operates in the frequency domain across the full bandwidth rather than sending a short pulse in the time domain. The instrument was light (~1.5 kg) and could be operated by a small rover. However, although the electronics unit was small enough (14.5 cm by 16 cm by 5.5 cm) to be easily accommodated inside the rover body, the polarimetric antenna system was bulkier and required its field of view to be free of any obstacle, which was challenging because of the inevitable presence of the rover's wheels. In the frame of this project, because it was not realistic to consider building another GPR operating at lower frequencies, which would have allowed deeper penetration (at the expense of vertical resolution), the choice was, therefore, made to use the prototype available as it was.

The payload cube

The payload cube was an independent perception device carried and launched by LUVMI-X to generate a 3D map of the skylight (Fig. 1B). It was equipped with two Intel Realsense D435 RGB-D cameras, used for the extraction of three local point clouds, and an Intel Realsense T265 to perform visual inertial simultaneous localization and mapping (SLAM) and to produce an estimation of the motion of the cube during the descent. This information was processed by an NVIDIA Jetson Nano, and a digital video transceiver, DTC-SOL8SDR-C, was used as an IP mesh communication module. The payload cube's Jetson Nano was equipped with Linux OS and the Robot Operating System framework to interface with the sensors, record the sensor data, and transmit it to LUVMI-X while descending for further forwarding to the CMS. Power was supplied by a 14.8-V, 2.6-Ah rechargeable Li-ion battery pack together with a DC-to-DC converter to stabilize the voltage supply to the devices at 12 V. The cube structure was 3D printed in polylactide with six panels and a central structure as mounting support for internal components. For space constraints, it was necessary to use flexible connectors. The total weight of the integrated device was 1.2 kg.

The available space for payloads on the LUVMI-X front panel allowed a launcher mechanism with a diagonal opening of 11.59 cm. This presented a major challenge in the design of the cube, having a maximum cube size of 8.2 cm per side with a volume of 551 cm^3. The T265 camera had a length of 10.8 cm, so it was placed on the diagonal of the bottom face of the cube. The two D435 cameras were placed on two opposite side faces of the cube to cover the major field of view of the skylight walls while descending. Another challenge was related to heat dissipation. The main heating component is the SOL8SDR-C, being an FPGA, which, together with Jetson Nano, produced a notable amount of heat to dissipate. To do so, two small fans were added to the system, guaranteeing the airflow necessary to keep the temperature lower than critical levels.

Tether management and docking subsystem

The TMDS was designed to enhance the heterogeneous robotic team capabilities when exploring rough terrain, especially steep or vertical walls. It linked two rovers via a tether using space robotic standard interconnects (see Fig. 1B). During the field tests, Coyote III descended the cliff of a skylight, whereas SherpaTT served as a cooperative anchoring point. Movie 2 (02:45) shows how this process was done. To minimize wear on the tether cable through friction against the surfaces while rappelling, the designed solution unrolls the tether from Coyote III. The integrated tether could be spooled and unspooled with an active winch, and a force sensor monitors the tether tension to avoid entanglement or slip. Besides providing a mechanical connection, the tether ensured power and data transmission between both rovers. The height of the TMDS platform could be adjusted through a parallel lifting mechanism, enabling docking with rovers of different heights and facilitating transport.

In more detail, the tether used was a 30-m off-the-shelf underwater cable, because it was not the aim to improve existing tethers for space applications (*28*). The winch was composed of a Robodrive ILM 70x18 motor and Harmonic Drive CSD-32-2A-160 strain wave gearing. For the lifting mechanism, two Robodrive ILM 38x12 motors were working in parallel as prismatic joints. Each motor was attached to a flanged ball screw nut on a rolled ball screw spindle with a 2-mm pitch. All three actuators were controlled with a brushless direct current motor driver stack (*29*). The built-in force sensor was a tension compression load cell (manufacturer, Burster; model, 8435-6002). The device comprised two different space robotic interfaces: a passive electromechanical interface (*30*) at the end of the tether and a passive HOTDOCK (*31*) at the top side of the platform. Thus, any robot equipped with the active counterpart of this interface and compatible dimensions could connect to the TMDS. In addition to the described interfaces, the system offered wireless connection via a 2.4-GHz mobile access point, enabling the TMDS to act as a communication relay. The TMDS did not feature a battery and hence had to be powered externally through one of the interfaces. Its total weight, including the onboard tether, was 23 kg. The TMDS measured 920 mm by 520 mm by 87 mm (length by width by height) in the folded state, and its height could be increased up to 300 mm in the extended state.

Mission management

The system was endowed with onboard real-time task planning, coordination, execution, and monitoring capabilities through the mission management subsystem. Hence, the mission was fully autonomous with command from the CMS in E4 autonomy mode (*32*) (i.e., goal commanding). This mission management subsystem tailored the European Robotic Goal-Oriented autonomous controller framework (*33*) at the mission level for collaborative phases (MP-1 and MP-3) by decomposing and coordinating the individual activities and at the robot level for specific activities (e.g., MP-3 parallel rappel and support rappel). Additionally, the subsystem monitored and detected nonnominal situations in execution, applying contingency actions when necessary. An example of contingency was automatically downgrading the autonomy level to telecommanding in case of failure and awaiting instructions from the CMS. All the activities were executed in real time, with the subsystem ensuring their timely execution. Upon detecting any deviation, the system replanned onboard and updated the execution such that the mission goals were achieved.

Figure S5 illustrates how the different subsystems interacted (i.e., functional chains) to achieve the MP-1 and MP-3 mission goals

from ground commanding to a successful execution. In the case of MP-1, the CMS commands ExploreArea, which is decomposed onboard by the mission management in three parallel goals to explore with the defined area. The agent of each robot decomposed the area in several equidistant points and planned the activities to explore them: takepictureat for Sherpa that included goto and then taking the image with the camera, takegprat for Coyote that included goto and then measure with the GPR, and traverse for LUVMI-X that included goto. In the case of MP-3, the CMS commanded Descent-Coyote, which is decomposed as DeployTMDS, followed by Dock-TMDS, followed by three parallel goals: SupportRappel, Rappel, and TrackRappel, one for each robot accordingly. The agent of each robot planned the goals and requested their execution via the corresponding system, in this case a one-to-one mapping.

Navigation: Perception and localization

The perception and localization subsystem was a core part of the autonomous system. From various propioceptive and exteroceptive sensor data, the subsystem could output the rovers' localization at 5 Hz and 2.5D terrain models as DEMs on request.

The subsystem was designed with modularity and versatility in mind so that it could easily be integrated on each rover with their own sets of sensors. 3D poses were required by the mission management to supervise the rovers' behavior and by the control subsystem for trajectory following. To be able to provide accurate localization at this high frequency, the subsystem relied on the fusion of various data sources such as wheel odometry, visual odometry, and IMU. Fusion was performed through factor graph optimization (*34*). Unlike Kalman filters, factor graphs were more flexible and could easily integrate different types of sensor data with various frequencies. Moreover, the incremental smoothing and mapping (iSAM2) method could achieve real-time performance and output an improved localization at required frequencies (*35*). In our implementation, wheel odometry poses were used as a variable to estimate, whereas other sensor data were integrated as constraint factors. Output localization was provided relative to the initial pose given in the mission frame. The system internally included a module keeping track of the rover frames on the basis of its geometrical model and regular joint state updates.

The perception chains designed to supply the visual odometry and DEMs included rectified frame pairs and disparity map production. In the case of stereo cameras, rectification was first performed on the raw camera images. For SherpaTT, calibration parameters were determined beforehand using a checkerboard, whereas the parameters from factory calibration were used for LUVMI-X. For Coyote III, disparity was directly computed from the depth provided by the cameras, and infrared frames were given to the visual odometry as input images. DEMs could be provided following the approach described in (*36*) as 2D matrices or point clouds as needed. On LUVMI-X and SherpaTT, a pan tilt unit was used to perform panoramic acquisitions and output a wider representation of the environment. To build the preliminary 3D map of the explored environment, each individual point cloud was stored with its metadata containing the estimated localization at the time of acquisition. It was then possible to merge all the consecutive point clouds at their known location to build the complete 3D map of the environment (see Fig. 5E).

Guidance and control

The vicinity of the skylight was explored in MP-1. For this purpose, 2.5D data served as input for the path planner to determine the optimal route to be followed by the robot team. The path planner was an adaptation of the fast marching method (*37*). This algorithm could extract a continuous, smooth, and globally optimal path to reach a goal within a given cost map of the scenario. In this regard, the cost map was generated by processing the local DEM of the terrain just in front of the rover, differentiating hard-to-traverse areas, obstacles, and safe areas.

On the control side, the trajectory follower ensured that the rover would follow the path. The chosen method was the conservative pure-pursuit, developed by the European Space Agency (*38*). It was able to follow a given path while maintaining the rover within a safe corridor. The follower parameters were tuned for each rover depending on their capabilities, considering their linear and rotational speeds as well as their turning limits given each particular locomotion type: full-Ackermann in SherpaTT and LUVMI-X and differential drive in Coyote III. Each rover had, additionally, a different locomotion controller in charge of translating the reference linear and rotational speeds from the trajectory follower into commands for the wheel (and steering) actuators, depending on the kinematic configuration of the rover (wheel poses with respect to the rover's inertial reference frame). In the case of SherpaTT, the locomotion also included a terrain-adaptive joint control algorithm to ensure stability and safe distribution of the weights when traversing uneven terrain (*17*).

Skylight 3D representation

The sensors of the payload cube provided two local 3D dense point clouds, together with an odometry and inertial measurements estimation coming from a visual SLAM module and an IMU, which comprised pose estimation, linear and angular velocities, and linear accelerations. The point cloud that was produced was purely geometrical because of computational limitations in the OBC. The sensor data recorded during the descent of the payload cube were directly transmitted to LUVMI-X.

On the rover, a mapping pipeline was executed to process the data into the final reconstruction. The first step was the data preprocessing: aligning the point clouds to a common frame. A filtering procedure based on voxel downsampling (*39*) was then applied to downsample all the dense local point clouds, with the double objective of removing noise and making further computations lighter. Furthermore, the radius outlier removal algorithm (*40*) was applied to reduce the number of points at an abnormal distance from their neighbors. The local 3D maps were then aligned to a global map using a combination of the ICP (*41*) algorithm and the previously computed odometry. A score was assigned to the alignment through ICP, and, if not performing above an empirical determined threshold, the transformation from the odometry computed via SLAM was used. A final refinement step was applied using the aforementioned filtering techniques.

The final result of this pipeline was a set of 3D points geometrically aligned to a fixed frame. On the basis of this information, the mesh reconstruction was created using the Alpha Shapes algorithm (*42*). From this reconstruction, it was possible to extract qualitative information regarding the skylight and visualize potential Coyote III ingresses into the lava tube.

Cooperative rappelling

Performing the autonomous rappelling operation of MP-3 was challenging considering that any misbehavior in the movement of the

robots could lead to a fatal failure for the two main systems involved: Coyote III as the rappelling robot and SherpaTT as the mobile anchor. Hence, to increase the safety of the mission, the cooperative rappelling component aimed to control both systems during the descent to minimize the tension that the tether applied to them.

The weakest point of the SherpaTT robotic arm was the spherical wrist. The wrist joints were capable of enduring forces but are not designed to resist high torques. As a result, these joints yielded whether the torques were large, which only happened during the rappelling if there was a substantial misalignment between the directions of the tether and the last link of the arm. The wrist torques could thus be eliminated by aligning the arm with the tether. This was the goal of the mobile manipulation component, which was divided into two control loops. First, the goal commander received the measurements of the force/torque sensor placed at the arm's end effector to compute a goal pose for the end effector that would compensate them, i.e., it tried to align the last link of the manipulator and the tether. Second, a MPC based on an optimal motion planner (*43*), which took the goal end effector pose as input, computed an optimal actuation for the system's joints to reach the goal and actuated the real system. In this regard, the MPC actuated both the mobile base and the manipulator joints to reach the goal end effector pose, although the mobile base movements were restricted to be parallel to the skylight to avoid the rover getting too close to it. This double control loop made mobile manipulation fast enough to react to changes in the tension of the tether. After deploying the TMDS, the SherpaTT manipulator kept the pose aligned with the TMDS until the rappelling started, so mobile manipulation is always initialized in a predefined, safe configuration.

On the other hand, regarding Coyote III, a small tension could lead to abrupt pulls from the rover once the vertical descents started. However, a high tether tension could induce slippage or even sinkage of the rover wheels when approaching the skylight. Controlling the tension applied to Coyote III at each stage of the descent was, hence, crucial for the mission's success. Intuitively, if the tether unwound slower than the driving speed of Coyote III, then the tension on the tether increased and vice versa. According to this rule, the tension was directly controlled by slightly modifying the unwinding speed of the tether depending on the measured and desired tether tensions with a simple proportional controller. The core of the rappelling operation was described in four states: traversing horizontally, traversing high incline, traversing vertically, and landing. Transition back and forth over these was based on the rover's pitch. Each of the states had reference speed and tension, which were set experimentally, i.e., low tension when the rover was still approaching the skylight and high tension when the rover was about to start descending vertically.

Statistical analysis

Before the field testing campaign, KPIs to quantitatively measure the effectiveness of the proposed approach were identified, and repetitions of the different MPs were planned to reach statistical significance on the studied KPIs. Given the large dimension of the overall mission, the limitations in resources and the difficulties involved in field testing (e.g., weather and limited communications), it was not possible to perform all the planned repetitions. Table S2 contains the different KPIs derived from the results obtained in the field test campaign.

In MP-1, the analysis focused on the reliability of the mission planning software, the GNC, and mapping capabilities. The most promising KPI of MP-1 was the relative localization error of LUVMI-X, which laid below the 10-cm range for a traverse of nearly 45 m. The MP-2 was the most repeated test; the KPIs focused mainly on communication robustness. The absence of a ground-truth model of the skylight made a quantitative analysis of the 3D reconstructions impossible. The different parts of MP-3 were tested separately and repeatedly, and one fully integrated demonstration (including TMDS deployment, Coyote III docking with TMDS, cooperative rappelling, and Coyote III undocking in the lava tube) was done. The successful rappelling operations reached 80% in five repetitions. Last, in MP-4, the best analyzed performance was achieved in teleoperation mode, given that the rover navigated more than 200 m inside the lava tube through the different terrains without damage.

Supplementary Materials

The PDF file includes:

Figs. S1 to S5
Tables S1 and S2
Legend for movie S1

Other Supplementary Material for this manuscript includes the following:

Movie S1

REFERENCES AND NOTES

1. T. d. J. M. Sanguino, 50 years of rovers for planetary exploration: A retrospective review for future directions. *Rob. Auton. Syst.* **94**, 172–185 (2017).
2. V. Stamenković, L. W. Beegle, K. Zacny, D. D. Arumugam, P. Baglioni, N. Barba, J. Baross, M. S. Bell, R. Bhartia, J. G. Blank, P. J. Boston, D. Breuer, W. Brinckerhoff, M. S. Burgin, I. Cooper, V. Cormarkovic, A. Davila, R. M. Davis, C. Edwards, G. Etiope, W. W. Fischer, D. P. Glavin, R. E. Grimm, F. Inagaki, J. L. Kirschvink, A. Kobayashi, T. Komarek, M. Malaska, J. Michalski, B. Ménez, M. Mischna, D. Moser, J. Mustard, T. C. Onstott, V. J. Orphan, M. R. Osburn, J. Plaut, A.-C. Plesa, N. Putzig, K. L. Rogers, L. Rothschild, M. Russell, H. Sapers, B. Sherwood Lollar, T. Spohn, J. D. Tarnas, M. Tuite, D. Viola, L. M. Ward, B. Wilcox, R. Woolley, The next frontier for planetary and human exploration. *Nat. Astron.* **3**, 116–120 (2019).
3. F. Sauro, R. Pozzobon, M. Massironi, P. de Berardinis, T. Santagata, J. de Waele, Lava tubes on Earth, Moon and Mars: A review on their size and morphology revealed by comparative planetology. *Earth Sci. Rev.* **209**, 103288 (2020).
4. J. Haruyama, T. Morota, S. Kobayashi, S. Sawai, P. G. Lucey, M. Shirao, M. N. Nishino, "Lunar holes and lava tubes as resources for lunar science and exploration," in *Moon: Prospective Energy and Material Resources* (Springer, 2012), pp. 139–163.
5. R. J. Léveillé, S. Datta, Lava tubes and basaltic caves as astrobiological targets on Earth and Mars: A review. *Planet. Space Sci.* **58**, 592–598 (2010).
6. A. Arya, R. Rajasekhar, G. Thangjam, Ajai, A. K. Kumar, Detection of potential site for future human habitability on the Moon using Chandrayaan-1 data. *Curr. Sci.* **100**, 524–529 (2011).
7. C. Fishman, J. G. Bevilacqua, A. S. Hahn, C. Morgan-Lang, N. Wagner, O. Gadson, A. C. McAdam, J. Bleacher, C. Achilles, C. Knudson, M. M. Millan, D. M. Bower, M. Musilova, S. S. Johnson, Extreme niche partitioning and microbial dark matter in a Mauna Loa lava tube. *J. Geophys. Res. Planets* **128**, e2022JE007283 (2023).
8. S. Plank, A. V. Shevchenko, P. d'Angelo, V. Gstaiger, P. J. González, S. Cesca, S. Martinis, T. R. Walter, Combining thermal, tri-stereo optical and bi-static InSAR satellite imagery for lava volume estimates: The 2021 Cumbre Vieja eruption, La Palma. *Sci. Rep.* **13**, 2057 (2023).
9. M. Tranzatto, T. Miki, M. Dharmadhikari, L. Bernreiter, M. Kulkarni, F. Mascarich, O. Andersson, S. Khattak, M. Hutter, R. Siegwart, K. Alexis, CERBERUS in the DARPA subterranean challenge. *Sci. Robot.* **7**, eabp9742 (2022).
10. R. U. Sonsalla, J. B. Akpo, F. Kirchner, "Coyote III: Development of a modular and highly mobile micro rover," in *Proceedings of the 13th Symposium on Advanced Space Technologies in Robotics and Automation* (*ASTRA-2015*) (European Space Agency, 2015), pp. 1–8.
11. M. J. Schuster, M. G. Müller, S. G. Brunner, H. Lehner, P. Lehner, R. Sakagami, The ARCHES space-analogue demonstration mission: Towards heterogeneous teams of autonomous robots for collaborative scientific sampling in planetary exploration. *IEEE Robot. Autom. Lett.* **5**, 5315–5322 (2020).

12. P. Arm, G. Waibel, J. Preisig, T. Tuna, R. Zhou, V. Bickel, G. Ligeza, T. Miki, F. Kehl, H. Kolvenbach, M. Hutter, Scientific exploration of challenging planetary analog environments with a team of legged robots. *Sci. Robot.* **8**, eade9548 (2023).
13. B. J. Morrell, M. Saboia da Silva, M. Kaufmann, S. Moon, T. Kim, X. Lei, C. Patterson, J. Uribe, T. Stegun Vaquero, G. J. Correa, L. M. Clark, A. Agha, J. G. Blank, Robotic exploration of martian caves: Evaluating operational concepts through analog experiments in lava tubes. *Acta Astronaut.* **223**, 741–758 (2024).
14. I. A. Nesnas, L. Kerber, G. Sellar, T. Balint, B. Denevi, A. J. Parness, R. P. Kornfeld, M. Smith, P. McGarey, T. Brown, E. Sunada, K. A. Gonter, B. Hockman, P. Hayne, T. Horvath, J. B. Hopkins, A. E. Johnson, R. V. Wagner, Y. Cheng, A. G. Curtis, K. Zacny, M. Paton, K. V. Sherrill, Moon Diver: Exploring a pit's exposed strata to understand lunar volcanism. *Acta Astronaut.* **211**, 163–176 (2023).
15. L. Burkhard, R. Sakagami, K. Lakatos, H. Gmeiner, P. Lehner, J. Reill, M. G. Müller, M. Durner, A. Wedler, "Collaborative multi-rover crater exploration: Concept and results from the ARCHES analog mission," in *2024 IEEE Aerospace Conference* (IEEE, 2024), pp. 1–14.
16. P. McGarey, D. Yoon, T. Tang, F. Pomerleau, T. D. Barfoot, Developing and deploying a tethered robot to map extremely steep terrain. *J. Field Robot.* **35**, 1327–1341 (2018).
17. F. Cordes, F. Kirchner, A. Babu, Design and field testing of a rover with an actively articulated suspension system in a Mars analog terrain. *J. Field Robot.* **35**, 1149–1181 (2018).
18. G. H. Just, M. J. Roy, K. H. Joy, G. C. Hutchings, K. L. Smith, Development and test of a lunar excavation and size separation system (LES^3) for the LUVMI-X rover platform. *J. Field. Robot.* **39**, 263–280 (2022).
19. D. Plettemeier, W.-S. Benedix, R. Hahnel, C. Statz, M. Laabs, E. Zakutin, Y. Lu, V. Ciarletti, E. Brighi, A. A. Le Gall, I. Sall, E. Mas Sanz, A. Shestov, GPR field-tests on Svalbard – WISDOM on ExoMars, poster presented at AGU Fall Meeting 2022, Chicago, IL, 12 to 16 December 2022.
20. M. Manz, J. Hilljegerdes, A. Dettmann, F. Kirchner, "Development of a lightweight manipulator arm using heterogeneous materials and manufacturing technologies," in *Proceedings of the 11th International Symposium on Artificial Intelligence, Robotics and Automation in Space* (European Space Agency, 2012), pp. 1–8.
21. R. Domínguez, S. Arnold, C. Hertzberg, A. Böckmann, "Internal simulation for autonomous robot exploration of lava tubes," in *Proceedings of the 15th International Conference on Informatics in Control, Automation and Robotics Volume 2: ICINCO*, INSTICC (SciTePress, 2018), pp. 144–155.
22. B. Mildenhall, P. P. Srinivasan, M. Tancik, J. T. Barron, R. Ramamoorthi, R. Ng, NeRF: Representing scenes as neural radiance fields for view synthesis. *Comm. ACM* **65**, 99–106 (2021).
23. B. Fei, J. Xu, R. Zhang, Q. Zhou, W. Yang, Y. He, 3D Gaussian splatting as new era: A survey. *IEEE Trans. Vis. Comput. Graph.* **31**, 4429–4449 (2024).
24. Y. Herve, V. Ciarletti, A. Le Gall, C. Corbel, R. Hassen-Khodja, W. S. Benedix, D. Plettemeier, O. Humeau, A. J. Vieau, B. Lustrement, S. Abbaki, E. Bertran, L. Lapauw, V. Tranier, N. Oudart, F. Vivat, C. Statz, Y. Lu, S. Hegler, A. Hérique, The WISDOM radar on board the ExoMars 2022 Rover: Characterization and calibration of the flight model. *Planet. Space Sci.* **189**, 104939 (2020).
25. N. Oudart, V. Ciarletti, A. Le Gall, M. Mastrogiuseppe, Y. Hervé, W.-S. Benedix, D. Plettemeier, V. Tranier, R. Hassen-Khodja, C. Statz, Y. Lu, Range resolution enhancement of WISDOM/ExoMars radar soundings by the Bandwidth Extrapolation technique: Validation and application to field campaign measurements. *Planet. Space Sci.* **197**, 104939 (2021).
26. N. Oudart, V. Ciarletti, A. Le Gall, Y. Herve, E. Brighi, Retrieval of the ground dielectric permittivity by planetary GPR accommodated on a rover: Application to the estimation of the reflectors' depth by the WISDOM/ExoMars radar. *Planet. Space Sci.* **224**, 105606 (2022).
27. E. Brighi, V. Ciarletti, A. Le Gall, F. de Lamberterie, Y. Herve, N. Oudart, "Identifying heterogeneity sizes in the subsurface with WISDOM, the GPR of the ExoMars mission," in *Europlanet Science Congress 2022*, vol. 16 (EPSC, 2022); https://doi.org/10.5194/epsc2022-55.
28. P. McGarey, T. Nguyen, T. Pailevanian, I. A. Nensas, "Design and test of an electromechanical rover tether for the exploration of vertical lunar pits," in *Proceedings of the 41st IEEE Aerospace Conference* (IEEE, 2020), pp. 1–10.
29. J. Hilljegerdes, P. Kampmann, S. Bosse, F. Kirchner, Development of an intelligent joint actuator prototype for climbing and walking robots, paper presented at the 12th International Conference on Climbing and Walking Robots and the Support Technologies for Mobile Machines, Istanbul, Turkey, 9 to 11 September 2009.
30. W. Brinkmann, F. Cordes, F. Kirchner, "A robust electro-mechanical interface for cooperating heterogeneous multi-robot teams," in *Proceedings of the IEEE/RSJ International Conference on Intelligent Robots and Systems* (*IROS*) (IEEE, 2015), pp. 1732–1737.
31. P. Letier, T. Siedel, M. Deremetz, E. Pavlovskis, B. Lietaer, K. Nottensteiner, M. Roa, J. S. Garcia Casarrubios, J. L. Corella Romero, J. Gancet, "HOTDOCK: Design and validation of a new generation of standard robotic interface for on-orbit servicing," in *71st International Astronautical Congress, IAC 2020* (International Astronautical Federation, 2020), p. 60218.
32. European Congress for Space Standardization, "ECSS-E-70-11, Space engineering: Space segment operability" (2005).
33. J. Ocon, F. J. Colmenero, J. Estremera, K. Buckley, M. Alsonso, E. Heredia, J. Garcia, A. I. Coles, A. J. Coles, M. Martínez, E. Savaş, F. Pommerening, T. Keller, S. Karachalios, M. Woods, I. Dragomir, S. Bensalem, P. Dissaux, A. Schach, "The ERGO framework and its use in planetary/orbital scenarios," in *International Astronautical Congress, IAC 2018* (International Astronautical Federation, 2018), p. 46215.
34. F. Kschischang, B. Frey, H.-A. Loeliger, Factor graphs and the sum-product algorithm. *IEEE Trans. Inf. Theory* **47**, 498–519 (2001).
35. M. Kaess, H. Johannsson, R. Roberts, V. Ila, J. J. Leonard, F. Dellaert, iSAM2: Incremental smoothing and mapping using the Bayes tree. *Int. J. Robot. Res.* **31**, 216–235 (2012).
36. M. Post, A. Bianco, X.-T. Yan, A. De Maio, Q. Labourey, S. Lacroix, J. Gancet, S. Govindaraj, X. Martinez-Gonzalez, I. Dalati, R. Domínguez, B. Wehbe, A. Fabisch, F. Souvannavong, V. Bissonnette, M. Smisek, N. W. Oumer, L. Meyer, R. Triebel, Z.-C. Márton, "Infuse data fusion methodology for space robotics, awareness and machine learning," in *69th International Astronautical Congress, IAC 2018* (International Astronautical Federation, 2018), p. 46477.
37. J. R. Sánchez-Ibáñez, C. J. Perez-del-Pulgar, M. Azkarate, L. Gerdes, A. García-Cerezo, Dynamic path planning for reconfigurable rovers using a multi-layered grid. *Eng. Appl. Artif. Intel.* **86**, 32–42 (2019).
38. L. Gerdes, M. Azkarate, J. R. Sánchez-Ibáñez, L. Joudrier, C. J. Perez-del-Pulgar, Efficient autonomous navigation for planetary rovers with limited resources. *J. Field Robot.* **37**, 1153–1170 (2020).
39. Y. Xu, X. Tong, U. Stilla, Voxel-based representation of 3D point clouds: Methods, applications, and its potential use in the construction industry. *Autom. Constr.* **126**, 103675 (2021).
40. X. Ning, F. Li, G. Tian, Y. Wang, An efficient outlier removal method for scattered point cloud data. *PLOS ONE* **13**, e0201280 (2018).
41. F. Wang, Z. Zhao, "A survey of iterative closest point algorithm," in *2017 Chinese Automation Congress* (*CAC*) (IEEE, 2017), pp. 4395–4399.
42. B. Guo, J. Menon, B. Willette, Surface reconstruction using alpha shapes. *Comput. Graph. Forum* **16**, 177–190 (1997).
43. G. J. Paz-Delgado, C. J. Pérez-del Pulgar, M. Azkarate, F. Kirchner, A. García-Cerezo, Multi-stage warm started optimal motion planning for over-actuated mobile platforms. *Intell. Serv. Robot.* **16**, 247–263 (2023).

Acknowledgments

Funding: This work was supported by the European Commission under the H2020 project entitled: Cooperative Robots for Extreme Environments (CoRob-X) under grant agreement 101004130. **Author contributions:** R.D.: mission concept design, software, field test, and writing; C.P.-d.-P.: mission concept design and writing; G.J.P.-D.: software, field test, and writing; F.P.: software, field test, and writing; J.B.: software, field test, and writing; T.G.: field test, writing, and managing; I.D.: mission concept design, software, field test, and writing; V.C.: mission concept design, scientific instruments, field test, and writing; A.-C.B.: software and field test; L.C.D.: software, field test, and writing; F.K.: Supervision. **Competing interests:** The authors declare that they have no competing interests. **Data and materials availability:** All data needed to support the conclusions of this manuscript are included in the main text or Supplementary Materials. The data for this study have been deposited in the database Zenodo (DOI: 10.5281/zenodo.14611244).

Submitted 31 July 2024
Accepted 15 July 2025
Published 13 August 2025
10.1126/scirobotics.adj9699

Science Robotics

Cooperative robotic exploration of a planetary skylight surface and lava cave

Raúl Domínguez, Carlos Pérez-del-Pulgar, Gonzalo J. Paz-Delgado, Fabio Polisano, Jonathan Babel, Thierry Germa, Iulia Dragomir, Valérie Ciarletti, Anne-Claire Berthet, Leon Cedric Danter, and Frank Kirchner

Sci. Robot. **10** (105), eadj9699. DOI: 10.1126/scirobotics.adj9699

Science Robotics (ISSN 2470-9476) is published by the American Association for the Advancement of Science. 1200 New York Avenue NW, Washington, DC 20005. The title *Science Robotics* is a registered trademark of AAAS.